Neurobiology of Aging 79 (2019) 83–92

Contents lists available at ScienceDirect

Neurobiology of Aging

journal homepage: www.elsevier.com/locate/neuaging

Spatial gradients of healthy aging: a study of myelin-sensitive maps

Vyacheslav R. Karolis [a,b,*], Martina F. Callaghan [c], Chieh-En Jane Tseng [b,d], Thomas Hope [c], Nikolaus Weiskopf [c,e], Geraint Rees [f], Marinella Cappelletti [f,g]

[a] FMRIB centre, John Radcliffe Hospital, University of Oxford, Oxford, UK
[b] Institute of Psychiatry, Psychology, and Neuroscience, King's College London, London, UK
[c] Wellcome Trust Centre for Neuroimaging, UCL Institute of Neurology, London, UK
[d] Department of Radiology, Massachusetts General Hospital, Harvard Medical School, Charlestown, USA
[e] Department of Neurophysics, Max Planck Institute for Human Cognitive and Brain Sciences, Leipzig, Germany
[f] UCL Institute of Cognitive Neuroscience, London, UK
[g] Psychology Department, Goldsmiths University of London, London, UK

ARTICLE INFO

Article history:
Received 8 September 2017
Received in revised form 6 February 2019
Accepted 5 March 2019
Available online 12 March 2019

Keywords:
Aging
Gradient
Maturation
Myelin
Magnetization transfer

ABSTRACT

Protracted development of a brain network may entail greater susceptibility to aging decline, supported by evidence of an earlier onset of age-related changes in late-maturing anterior areas, that is, an anterior-to-posterior gradient of brain aging. Here we analyzed the spatiotemporal features of age-related differences in myelin content across the human brain indexed by magnetization transfer (MT) concentration in a cross-sectional cohort of healthy adults. We described age-related spatial gradients in MT, which may reflect the reversal of patterns observed in development. We confirmed an anterior-to-posterior gradient of age-related MT decrease and also showed a lateral-to-ventral gradient inversely mirroring the sequence of connectivity development and myelination. MT concentration in the lateral white matter regions continued to increase up to the age of 45 years and decreased moderately following a peak. In contrast, ventral white matter regions reflected life-long stable MT concentration levels, followed by a rapid decrease at a later age. We discussed our findings in relation with existing theories of brain aging, including the lack of support for the proposal that areas which mature later decline at an accelerated rate.

1. Introduction

Brain development is associated with asynchronous anatomical alterations in macrostructure and microstructure, with different regions maturing at different times and rates (Deoni et al., 2011; Gogtay et al., 2004; Sowell et al., 2004). In white matter (WM), corticospinal and thalamocortical connectivity, supporting basic sensory and motor functions, is the first to develop, followed by the proliferation of unilateral corticocortical connections once the thalamocortical connections have grown into the cortical plate (Kostovic and Jovanov-Milošević, 2006). Flechsig's Law of Myelogenesis (Flechsig, 1901) proposes that the sequence of myelination is linked to the development of functional systems. In support of this, a ventral-to-lateral gradient of maturation characterizes the process of axon myelination (Kinney et al., 1988; Yakovlev and Leours, 1967). Corticocortical connections are more likely to develop for longer as they play a critical role in supporting high-level adaptive behavior (Catani et al., 2012; Kinney et al., 1988). A protracted development of language networks (Gogtay et al., 2004; Sowell et al., 2003), with their left hemisphere dominance, may also explain greater postnatal myelin growth in the left compared with the right hemisphere in the posterior brain (Deoni et al., 2011).

How this asynchronous maturation across the brain might subsequently affect the process of aging remains an open question. One possibility is "last-in, first-out," that is, the temporal sequences of maturation and aging are inversely related (Douaud et al., 2014; Raz, 2000; Reisberg et al., 1999). While the exact mechanisms for this pattern are not known, it has been suggested that protracted development of a brain network, which may continue at least as late as the third decade from birth (Lebel and Beaulieu, 2011; Somel et al., 2009), would entail a greater exposure to adverse environmental factors and subsequently result in a greater susceptibility to

* Corresponding author at: Department of Psychosis Studies, Institute of Psychiatry, Psychology and Neuroscience, King's College London, 16 De Crespigny Park, Camberwell, London SE5 8AF, UK. Tel.: +44 1865222523; fax: +44 1865222717.
E-mail address: vyacheslav.karolis@ndcn.ox.ac.uk (V.R. Karolis).

0197-4580/$ – see front matter © 2019 Published by Elsevier Inc.
https://doi.org/10.1016/j.neurobiolaging.2019.03.002

aging decline (Casey et al., 2000). Changes in the regenerative abilities of the brain may also play a role. For example, monkey studies suggest that despite a continued production of myelin in aging monkeys, the sheaths of myelin formed later in development are easier to break down (Peters et al., 2001) and therefore less stable.

In line with this "last-in, first-out" (retrogenesis) principle, gray matter volume in late-maturing prefrontal regions typically starts declining earlier than in posterior regions (Davis et al., 2008; Gogtay et al., 2004; Raz et al., 1997, 1998). An anterior-to-posterior gradient of aging also emerges in WM microstructure, with greater fractional anisotropy (FA) (Basser et al., 1994) decreases observed in the prefrontal WM and in the anterior part of the corpus callosum compared with posterior areas (Salat et al., 2005a, b).

The existing evidence does not, however, support the retrogenesis perspective unambiguously. For example, phylogenetically old medial temporal regions which mature early, like the hippocampus and entorhinal cortex (Gogtay, 2004; Shaw et al., 2008), nevertheless show accelerated volume shrinkage with age (Fjell et al., 2014; Raz et al., 2005, but see; Bigler et al., 1997) and have been implicated in neurodegenerative disorders (Schmitz et al., 2016; West et al., 1994). FA also decreases in the cerebral peduncles and in the posterior limb of the internal capsule containing early-myelinating fibers of the corticospinal tract (Brickman et al., 2012; Salat et al., 2005a, b).

Two views of retrogenesis can be further distinguished. One focuses on the spatial layout of age-related changes and assumes greater differences between young and older adults in the later maturing regions as a result of an earlier onset of aging (e.g., Head et al., 2004). The other view instead emphasizes the dynamic features of aging by proposing that later maturing brain areas are characterized by an accelerated rate—not by an earlier onset—of decline (Bender, Vö;lkle, and Raz, 2016; Douaud et al., 2014; Sexton et al., 2014).

In WM aging research, these inconsistent findings may result from the limited specificity of FA measures (Deoni et al., 2008; Jones et al., 2012), as various factors contributing to FA may be differentially affected by aging. For instance, myelin is just one of at least 4 major contributors to the FA signal (Jones et al., 2012), with the sensitivity of FA to crossing fibers, complicating the interpretation of any local increases or decreases (Douaud et., 2011). Therefore, it is not clear whether the "last-in, first-out" principle is applicable to age-related myelin changes. The issue may be resolved by exploiting a more detailed characterization of microstructural content, which may in turn also reveal new spatial gradients of aging beyond the anterior-to-posterior gradient, as predicted from developmental studies (Deoni et al., 2011; Kinney et al., 1988; Kostovic and Jovanov-Milošević, 2006; Yakovlev and Leours, 1967).

In the present study, we capitalized on the past developmental findings to test specific predictions concerning the spatial and temporal features of age-related differences in WM. We collected magnetization transfer (MT) saturation maps (Helms et al., 2008; Weiskopf et al., 2013) in a large cross-sectional sample of adults. MT maps show high correlations with myelin content measured histologically (e.g., Schmierer et al., 2007). Given the cross-sectional character of the data, the present study refers to "age-related differences" to denominate the individual variability that is collinear with a participant's age. We hypothesized that in addition to an anterior-to-posterior spatial gradient of healthy aging, other gradients, such as a left-to-right and a lateral-to-ventral, may emerge as a reflection of the asynchrony in structural brain development. By analyzing the patterns of age-related differences, we also sought to investigate any temporal features of aging whereby regions that reach a maturation peak late may show an accelerated rate of change of age-related differences following the peak.

2. Methods

2.1. Participants

Ninety-seven healthy high-functioning participants without neurological or psychiatric disease and with no contraindications to magnetic resonance imaging (40 males, 57 females; mean age: 46.4, age range: 20-74) provided written informed consent to take part in the magnetic resonance imaging study approved by the local ethics committee. All participants above the age of 34 years received the Mini-Mental State Examination (Folstein et al., 1975) and achieved a score of 27 or greater, suggesting that their cognitive faculties were within the normal range. Four aging participants reported taking medications for either hypertension or high cholesterol. None of the participants reported being diabetics. See Table 1 for a summary of the participants' demographic features.

2.2. Data acquisition

All participants were scanned using the same protocol and hardware. A whole-brain quantitative multiparameter mapping protocol implemented at the Wellcome Trust Centre for Neuroimaging in London was used on a 3T whole body MR system (Siemens Healthcare, Erlangen, Germany) equipped with a standard 32-channel head coil for receive and radiofrequency transmission. Following an established paradigm (Callaghan et al., 2014; Lutti et al., 2010, 2012; Weiskopf et al., 2013), the multiparameter mapping protocol consisted of 3 spoiled multiecho 3D fast low angle shot acquisitions with 1 mm isotropic resolution and 2 additional calibration sequences to correct for inhomogeneities in the RF transmit field. The fast low angle shot volumes were acquired with predominantly proton density (PD*) or T_1 weighting, as determined by the repetition time and flip angle combination. MT weighting was achieved through the application of an off-resonance pulse before excitation. Quantitative MT saturation was calculated from the acquired images using an in-house MATLAB program. The method has been previously shown to inherently account for inhomogeneities of the receive coil and the transmitted RF field (Helms et al., 2008). The relationship of magnetization transfer signal to the content of myelin has been previously demonstrated in histological studies of ex vivo multiple sclerosis patients and animal models (Ou et al., 2009; Schmierer et al., 2007, 2008).

2.3. Image coregistration

The preprocessing pipeline is shown in Fig. 1. To improve the separation between brain and nonbrain tissues in MT maps, nonbrain tissues were masked out using participants' T1-weighted and PD* maps (Callaghan et al., 2014), linearly coregistered with MT

Table 1
Demographic features of the participants

Participants	Gender	Mean age (SD)	Years of education (SD)	MMSE (median and range)	Handedness
Young ($n = 29$)	11M, 18F	26.4 (4.7)	17.6 (2.1)	NA	1 L, 28 R
Middle ($n = 38$)	17M, 21F	46.6 (6.7)	17.1 (3.2)	30 (27-30)	3 L, 35 R
Older ($n = 30$)	12M, 18F	65.9 (4.3)	16.0 (2.9)	30 (28-30)	3 L, 28 R
Total/ mean	40M, 57F	46.3 (5.2)	16.9 (2.7)	30 (28-30)	7 L, 91 R

Key: F, females; L, left; M, males; MMSE, Mini-Mental State Examination; NA, not applicable; R, right; SD, standard deviation.

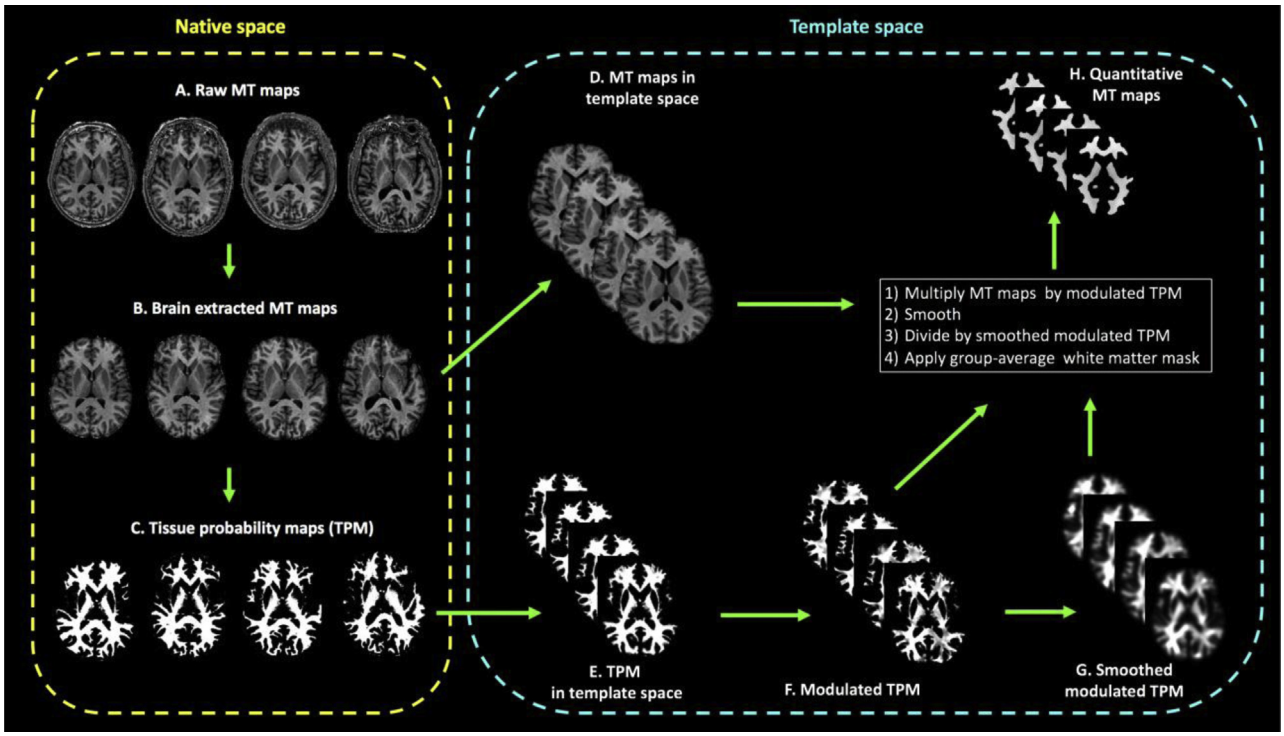

Fig. 1. Preprocessing pipeline. Abbreviations: MT, magnetization transfer; TPM, tissue probability map.

maps. Brain extraction implemented in FMRIB Scientific Library Brain Extraction Tool was performed on T1-weighted and PD* maps, and the 2 masks outputted by this process were used to create a common Boolean AND brain mask. Individual MT maps were multiplied by the mask and were once again submitted to BET using a low value for the fractional intensity threshold *f* for an additional cleanup of the nonbrain tissues. The results were visually checked for quality and manually adjusted for incorrectly excluded brain voxels.

A study-specific whole-brain template and diffeomorphic transformations between native and standard spaces were generated using the Greedy symmetric diffeomorphic normalization Greedy SyN pipeline distributed with the Advanced Normalization Tools (http://stnava.github.io/ANTs; Avants et al., 2011), a joint top-performing normalization method among 14 common methods (Klein et al., 2009). Once an initial affine template was created, 4 iterations of the nonlinear refinement were performed. The template was coregistered linearly with the ICBM152 MNI template.

2.4. Calculation of standardized quantitative maps

The standardized quantitative maps were obtained using the procedure outlined in Draganski et al., (2011), which is a modified version of the T-SPOON algorithm proposed in Lee et al., (2009). After this method, tissue-specific parameter maps are produced while optimally preserving the quantitative parameter values within each tissue class and reducing effects of residual misregistration and partial volume effects (Draganski et al., 2011; Lee et al., 2009). The following steps were performed. First, gray matter and WM tissue probability maps (TPMs) were obtained from the MT maps in native space using the unified segmentation approach implemented in SPM12. The TPMs were then warped into the standard space and scaled by the Jacobian determinants of the deformation field. A combined probability weighting and Gaussian smoothing (using a 6 mm full width at half maximum isotropic smoothing kernel) was then applied to the WM quantitative maps, whereby each participant's quantitative maps in the standard space were, in exact order, multiplied by an unsmoothed modulated TPM, smoothed, and then divided by a smoothed modulated TPM (see Fig. 1). The use of modulated weighting before the application of the Gaussian filter is the main modification to the T-SPOON algorithm, allowing compensation for the effect of the individual variability in the brain size (Draganski et al., 2011) (the effect of modulation is then undone by dividing with the smoothed modulated images) and hence decreasing the partial volume effects. Finally, group-average masks were generated by thresholding individual probability maps for each tissue class at 0.2 and then averaging them across all participants. Each voxel was subsequently assigned to a tissue class for which an average probability value was maximal. This approach was used to ensure that each voxel was analyzed in only one subspace (Callaghan et al., 2014). Intracranial volumes were calculated using procedure outlined in the study by Keihaninejad et al., 2010.

2.5. Statistical analyses

2.5.1. Outline of statistical approach

Statistical analyses were run in 3 stages. In the first stage, we identified WM regions showing significant age-related effects and separated linear patterns of age-related differences from nonlinear patterns. For this purpose, we used polynomial fits up to a 3rd order as approximations to the trajectories of age-related differences and used model selection procedure to decide which of those best accounted for the data. In the second stage, we compared the inter-regional differences in age-related effects, including interhemispheric differences. In the third stage, we investigated spatiotemporal patterns of age-dependent differences, focusing only on the regions which showed nonlinear patterns. Specifically, given that aging is associated with demyelination, we aimed to estimate the point in the studied age-range at which MT starts decreasing at a rapid rate. This would serve as a cross-sectional estimate for the time

of the onset of age-related decline. For this purpose, we used piecewise linear approximations to nonlinear trajectories, provided by a two-component segmented fit. Additional details of the statistical methods are outlined below in Sections 2.5.2 and 2.5.3.

2.5.2. Construction of maps showing age-related effects

Mass-univariate statistical analyses of age-related effects in WM were carried out using a multiple linear regression model embedded in the general linear model framework of SPM12. To identify and characterize the spatiotemporal features of age-related changes, each voxel was fitted with 3rd order polynomial model using age as a linear, quadratic, and cubic predictor. There was a very moderate negative association between years of education and age, r = -0.18. Consequently, years of education, together with sex and intracranial volume, was entered as a variable of no interest. Omnibus F-contrast test for all predictors associated with age was run to create a map of significant age-related differences using threshold criterion of $p <$ 0.05 (familywise corrected). The map was then parcellated further into "linear" (linear predictor only), "2nd order" polynomial (both a linear and quadratic predictor), and "3rd order" polynomial model maps using likelihood ratio test at each individual voxel.

2.5.3. Inter-regional distributions of age-related effects

The strength of the age-related effects across WM was quantified using Cohen f^2 for the full model compared with the models containing only the parameters of no interest. Partitioning of WM into subdivisions was obtained by running FreeSurfer white matter parcellation onto the study template. Labeling of the WM regions was done using John Hopkins University tractography and ICBM-DTI-81 atlases distributed with FSL. To perform an analysis of the interhemispheric differences, MT maps were coregistered with a symmetrical MNI template (available at http://www.bic.mni.mcgill.ca/ServicesAtlases/ICBM152NLin2009). We then obtained the distribution of aging effects in each voxel in the symmetrical space by means of bootstrapping procedure, whereby we sample 1000 participants sets, randomly with replacement, and obtained the distribution of Cohen's f^2 for each voxel. We then split the effect size maps into the left and right hemisphere maps, flipped X-Y orientation of left hemisphere maps, and subtracted them from the corresponding right hemisphere maps. The voxels which showed a larger effect size in one of the hemispheres in 97.5% cases (i.e., approximating $p < 0.05$, two-tailed) and form clusters of more than 50 voxels were considered as showing significant lateralization of age-related differences.

2.5.4. Spatiotemporal patterns of age-related differences

In the further analyses of brain regions showing non-linear patterns, we sought to estimate (1) the critical points in the trajectory of age-dependent differences at which the gradients of these differences change and (2) the gradients of age-related differences preceding and following these points. For a detailed characterization of these properties, the two-component segmented (aka piecewise) linear fit (Toms and Lesperance. 2003), as implemented in the study by R Core Team, 2015, was applied to the voxels for which a nonlinear fit, either 2nd or 3rd order polynomial, outperformed the linear one. Before fitting, the data were residualized with respect to intracranial volume, years of education, and sex. Three parameters of interest characterize the segmented fit: (1) breakpoint, that is, a point that separates 2 linear segments of the fitted function; this parameter was used as an estimate for a critical point in the trajectory; the rate of change of the linear segment (2) before and (3) after the breakpoint. The latter 2 characterized how quickly the age-related differences unfold, before and after the critical point on the trajectory, respectively.

A correction of the parameter estimates was performed because the segmented linear fit has no analytical solution and can produce degenerate estimates of parameters if the algorithm minimizing the cost function stops at a local minimum. In the first step of this procedure, the parameters of interest were plotted for visual inspection to identify any cases of clear degeneracy which may have required refitting if necessary to obtain more appropriate estimates. These cases (1%) showed an estimated breakpoint close to the extrema of the studied age distribution, coupled with abnormal rate of change of the linear segment before or after the breakpoint. This effectively implies a linear trajectory of aging, which is not supported by the results of the model selection procedure. Next, for a further improvement of the estimates, the parameters of interest were spatially smoothed (Eklund et al., 2012) by mapping them onto the brain and by applying a Gaussian filter with full width at half maximum of 3 mm. Normalized convolution (Knutsson and Westin, 1993) was applied to prevent the effect of the voxels being outside the WM mask, with weights = 1 if a voxel was within WM mask and weights = 0 otherwise. After this procedure, the parameter estimates represented a weighted average of the parameters in the neighborhood of the voxel for which the parameter was estimated.

3. Results

3.1. Spatial distribution of linear and nonlinear patterns

The spatial extent of significant age-related differences and the best-fitting model maps are shown in Fig. 2. These differences, predominantly nonlinear, were bilateral in the frontal lobe. More posteriorly, regions showing significant age-related differences were found more frequently in the left than in the right hemisphere. In the left hemisphere, these age-related differences extended from the parietal lobe into both the occipital and the posterior part of the left temporal lobe. The corpus callosum was relatively unaffected with the exception of the anterior part (genu). Significant age effects did not spread into the anterior or ventral temporal lobes.

3.2. Effect size

Fig. 3A and B show the spatial map of age-dependent effect size across WM and its frequency distributions within WM parcels, respectively (also see Supplementary Fig. 1 for a high-resolution version of Fig. 3A) The strongest effect can be seen in the frontal lobes (Cohen's $f^2 = 0.70$, CI = [0.37 1.02]). The anterior-to-posterior spatial gradient can also be observed in WM parcels extending in the anterior-to-posterior direction. Thus, the insula, the cingulate (see Supplementary Fig. 2), and deep WM regions were characterized by bimodal distributions, with a stronger effect in the anterior subdivisions of these parcels. The weakest effects of aging were found in temporal (Cohen's $f^2 = 0.30$, CI = [0.13 0.56]) and occipital WM (Cohen's $f^2 = 0.27$, CI = [0.11 0.48]). Supplementary Fig. 3 illustrates that the strength of the age-dependent effects was unaffected by partialling out variances predicted by the PD* and R2* maps which are sensitive to WM pathology and neurovascular alterations, respectively.

The analysis of age-dependent lateralization effects identified 8 regions where these effects differed significantly between the left and right hemispheres (Fig. 3C). In the posterior brain, 5 WM regions showed greater age-dependent differences in the left than in the right hemisphere: one region anterior to the inferior half of the putamen (intersection of internal and external capsules); 2 regions in the occipital WM, one lateral and one medial; WM under the angular gyrus, likely to be part of arcuate fasciculus; a WM region situated deeply under the middle frontal gyrus. Age-related effects were stronger in the right hemisphere in 3 regions: 2 regions

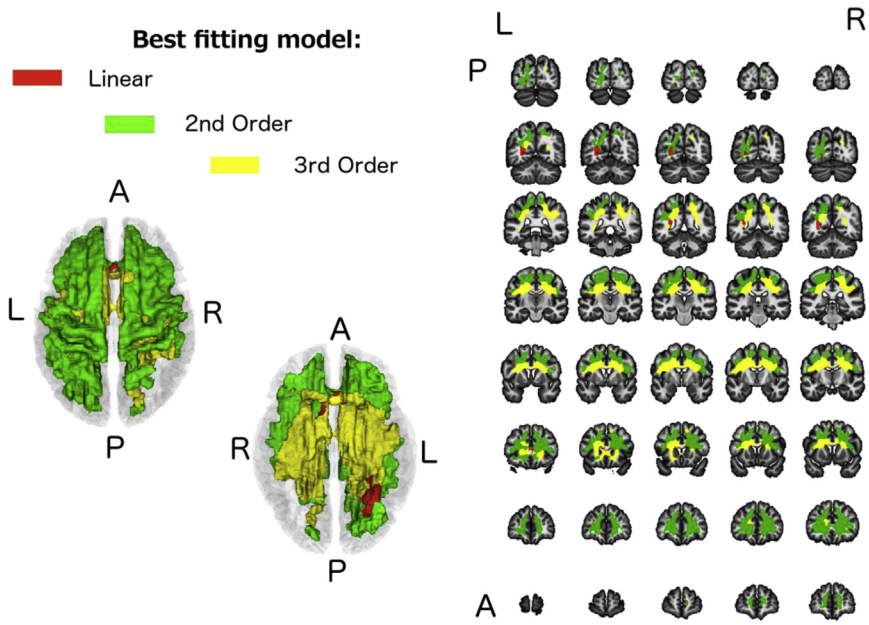

Fig. 2. Spatial distribution of significant linear and non-linear (2nd and 3rd order polynomial fits) age effects in white matter maps. Left panel: superior and inferior views. Right panel: coronal slices. Abbreviations: A, anterior; L, left; P, posterior; R, right.

underlying the inferior parts of the precentral and postcentral cortices and one region in the frontal lobe adjacent to the bottom of the cingulate sulcus.

3.3. Spatiotemporal characteristics of the age-related differences

The results of polynomial fitting suggest distinct spatiotemporal patterns of age-related differences in lateral and ventral WM. The analyses using segmented linear fitting demonstrate this point in greater detail. The spatial maps of the segmented fit parameters in the WM are shown in Fig. 4 (also see Supplementary Figures 4-6 for high resolution maps of each parameter) and examples of these fits superimposed over polynomial fits in Fig. 5A(i)-(iii). The distribution of segmented fit breakpoints, which is bimodal in its form (Fig. 5B [i]), reveals a lateral-to-ventral gradient, such that earlier breakpoints, occurring at around 45 years of age, are found in lateral areas of WM, whereas later breakpoints, occurring at around 58 years of age, are found in ventral areas. The earliest breakpoints (around 37 years of age) could be observed in the left occipital and bilateral orbitofrontal WM regions, overlapping with posterior and anterior segments of inferior fronto-occipital fasciculus, respectively. Breakpoint values were associated with the rate of change of age-related MT differences before and after the breakpoint (Fig. 5B [ii]-[iii]). More lateral regions, especially the frontal areas, showed a continued MT increase before an early breakpoint (rate of change before breakpoint >0), followed by a decrease at a relatively slow rate. Conversely, deeper and more ventral WM areas showed no MT increase (rate of change before breakpoint ≈ 0) up to a later stage, followed by a decrease at a rapid rate. In all trajectories, the rate of change after the breakpoint was always negative, indicating that no region showed an MT increase after the trajectory bending. There was a positive association between the breakpoint and the strength of the mean (across-participants) MT intensity ($r = 0.54$), indicating that later breakpoints occurred in regions with more MT concentration.

Given that a linear approximation to the trajectory after breakpoint may conceal its curvilinearity, we also considered a more refined approximation for those brain areas which demonstrated an early (less than 52 years) breakpoint. The analysis aimed to determine whether there was an actual difference at an older age range between the rate of change of the trajectory describing age-related differences in the more lateral voxels showing an early breakpoint and the rate of change in regions associated with a later breakpoint. For this purpose, we refitted the segmented fit to these voxels, considering only participants whose age was greater than the estimated breakpoint. The segmented fit converged to the values which were not at the extremes of the fitted age range in 41% of voxels. For the voxels that did not converge, we fitted a simple linear regression based only on participants who were 52 years old and older (38 participants). As Fig. 5C suggests, the voxels where the segmented fit converged show a rate of change more similar to voxels with a late breakpoint. This was not the case for the voxels without convergence. Across all WM voxels, the rate of change at an older age range was negatively associated with the average across-subjects MT intensity, $r = -0.42$ (Fig. 5D–I). Importantly, their association was strictly proportional: after dividing the rate of change by the average across-sample MT intensity, this association completely disappears, $r = -0.03$ (Fig. 5D [ii]).

3.4. Comparison of a one-breakpoint model fit to a two-breakpoint fit

Finally, we considered whether one-breakpoint (two-component) segmented fit may not have been sufficient to model critical points on the trajectory describing age-related differences. We compared one-breakpoint model's goodness of fit to a two-breakpoint (three-segment) model's using Akaike Information Criterion. The analysis revealed 2 areas where a two-breakpoint model outperformed the one-breakpoint model (Fig. 6A): one was located in the deep WM of superior corona radiata, overlapping considerably with the path of the corticospinal tract; the other, of a considerably smaller extent, was observed in the orbitofrontal WM, in the proximity of regions showing the earliest breakpoint for the one-breakpoint model, but not overlapping with them. Both patterns were left-hemisphere dominant but differed in their temporal features (Fig. 6B). For the deep WM region, MT decreased until the age of 32.6 years on average, followed by an increase until the age of

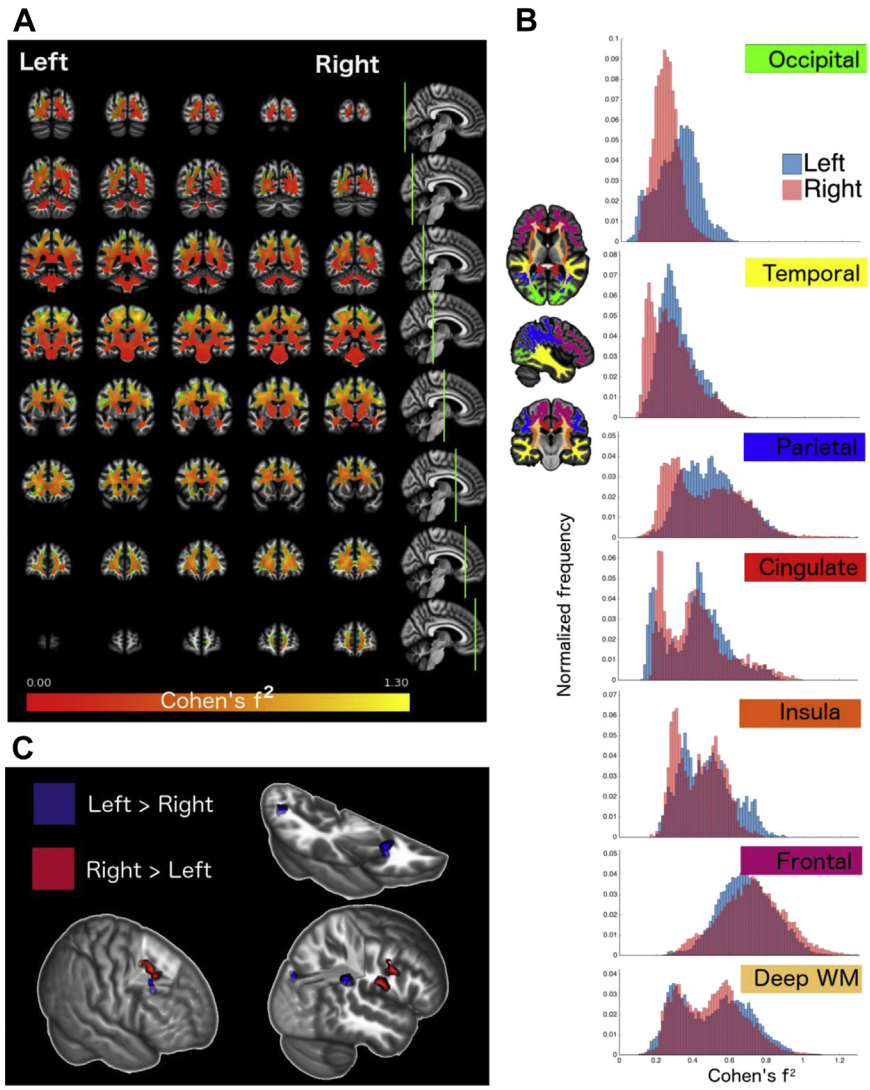

Fig. 3. Age-related effect size (A) Spatial map of effect sizes. Location of the coronal slices shown on the right refers to the (adjacent) rightmost column of the spatial maps. The green edge encircles the areas where the effect of aging was significant (as shown in Fig. 2). (B) Distribution of effect sizes in white matter parcels. (C) Locations of significant differences in effect size between left and right hemispheres. The title of each histogram is color-coded relative to the white matter parcel, as shown in the brain's map. Abbreviation: WM, white matter. (For interpretation of the references to color in this figure legend, the reader is referred to the Web version of this article.)

57.7 years on average, and then followed by a decrease. In the orbitofrontal area, MT increased before the first breakpoint (at the mean age of 28.1 years) followed by a shallow decrease till the second breakpoint (at the mean age of 60.2 years), and then followed by a decrease.

4. Discussion

In the present study, we investigated the temporal and spatial features that characterize age-related differences in myelin-sensitive MT maps in a cross-sectional cohort of adults ranging from 20 to 74 years old. Widespread age-dependent alterations in such maps have previously been reported (Callaghan et al., 2014), but their spatiotemporal properties have not yet been characterized. Using evidence from developmental studies (Deoni et al., 2011; Kinney et al., 1988; Kostovic and Jovanov-Milošević, 2006; Yakovlev and Leours, 1967) and on the basis of the "last in, first out" principle, we predicted that a detailed analyses of the trajectories describing age-relative differences in the myelin-sensitive maps may reveal lateral-to-ventral and left-to-right spatial gradients of healthy aging, in addition to an anterior-to-posterior gradient.

As predicted, we found widespread age-related MT decrease in the frontal lobe. Given that changes in MT contrast are associated with increases/decreases in myelin content (Ou et al., 2009; Schmierer et al., 2007, 2008), these findings suggest a particular sensitivity of frontal myelin to the effect of aging as compared, for instance, to occipital myelin. Furthermore, WM parcels, which extend in the anterior-posterior direction, namely the deep WM and regions under the insular and cingulate cortices, revealed bimodal distributions of effect size with more age-affected regions situated frontally. The main deviation from this pattern was the parietal MT where a considerable number of voxels showed a significant age-related effect. This is however not surprising, given that frontal and parietal regions are organized into functional systems involved in higher cognitive abilities, such as working memory (Owen et al., 2005); according to the Flechsig's Law (Flechsig, 1901), the developmental changes of functionally coupled anatomical regions proceeds in parallel. Interestingly, our results showed a rather moderate aging effect in the temporal lobe, consistent with some previous

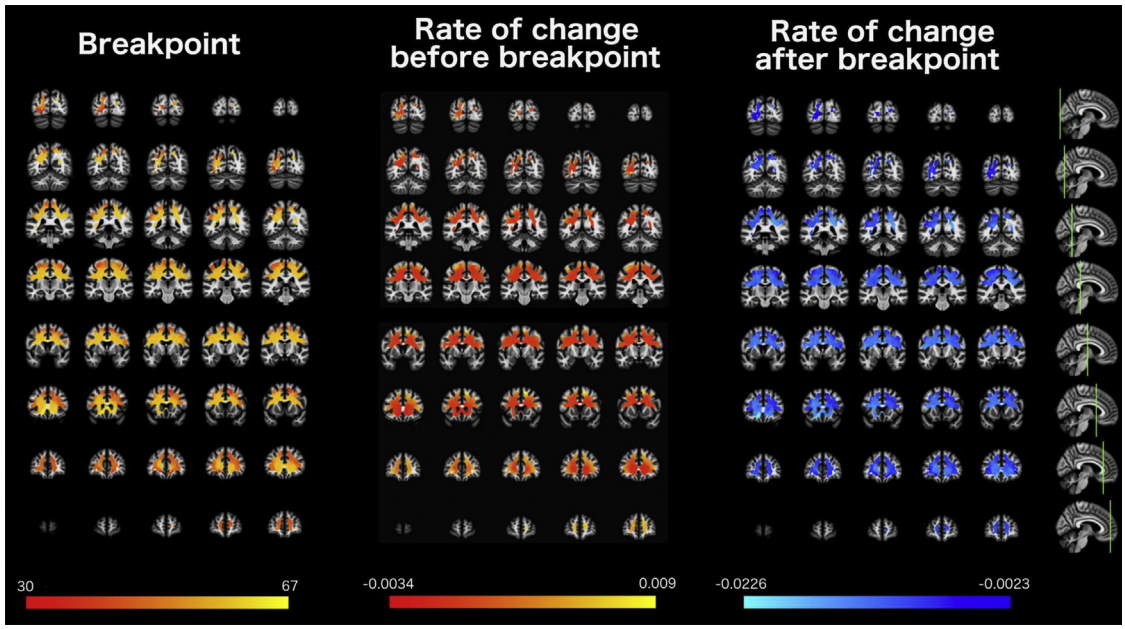

Fig. 4. Spatial maps of the parameters of the segmented fit. Location of the coronal slices shown on the right refers to the rightmost columns of the spatial maps (for higher resolution images—see Supplementary Figures S4-S6).

reports (Sexton et al., 2014) and suggesting that brain regions showing myelin loss in healthy aging are topographically different from the areas where neurodegeneration occurs (e.g., Huang et al., 2007; Sturm et al., 2013; Wisse et al., 2014).

There was no sufficient evidence for a left-to-right gradient of aging in WM myelin. Previous studies suggested that language networks, with their (typically) left hemisphere lateralization, develop for longer (Gogtay et al., 2004; Sowell et al., 2003). In line with these results, a hemispheric asymmetry has also been shown in postnatal changes in parietal, temporal, and occipital myelin-sensitive maps (Deoni et al., 2011), suggesting that age-related differences myelin may be more pronounced in the left hemisphere. We found a wider spread of statistically significant differences in the posterior left hemisphere. However, a direct comparison with the right hemisphere showed only local differences in the strength of age-related effects. These differences are difficult to interpret due to known limitations in the voxelwise precision of WM regional alignment. Future research could benefit from integrating imaging modalities assessing myelination with diffusion-weighted imaging to provide a more accurate anatomical delineation of WM structures.

Finally, the analysis of the temporal properties of the trajectories describing age-related differences revealed a lateral-to-ventral gradient. The age-related decrease in MT occurred earlier in lateral areas of WM, likely to be dominated by corticocortical connection, relative to ventral areas, which are dominated by thalamocortical connections and fibers of corona radiata. In support of this, there was a positive association between the breakpoint and the strength of the mean (across-participants) of MT intensity, suggesting that the myelin-rich areas are more likely to have a late breakpoint. The lateral WM regions followed a "growth–peak–decline" trajectory, with a peak occurring at around 45.5 years, followed by a relatively slow rate of age-related differences. In contrast, ventral WM areas showed relatively stable MT levels till a later stage (around late 50s), suggesting that these areas matured earlier than the age range we studied. The late breakpoint in these areas was followed by a rapid rate of change in age-related differences.

We also note that our results challenge the proposal that late maturing regions decline at an accelerated rate (e.g., Bender, Völkle, and Raz, 2016; Douaud et al., 2014) when this refers to age-related differences identified by myelin-sensitive WM maps. Areas with an early breakpoint showed a moderate rate of MT decrease compared with areas with a later breakpoint. A more detailed analysis focusing on the later age range demonstrated that these rates were strictly proportional to the average voxelwise MT concentration; that is, at a later age, the rate of MT decrease was equal across regions showing significant age-related differences once the voxelwise concentration was taken into account. This suggests that the defining factor is the presence of a proportional relationship between MT concentration and its age-dependent decrease rather than a greater vulnerability of the ventral regions to aging at a late age range. It is however possible that no evidence of an accelerated decline is due to sample differences. In the present study, participants had no known health issues and the upper age limit was younger than that in other studies (e.g., Douaud et al., 2014), thereby reducing the likelihood of having participants with subclinical manifestations of age-related pathologies, which may be related to an accelerated rate of age-related brain changes.

The results of the present study may help delineating temporal boundaries between the duration of maturation and the onset of aging. Animal studies showed that the adult-born oligodendrocytes continue to synthesize myelin, indicating that myelin genesis persists during adult life (Rivers et al., 2008). The exact time when maturation ends in the human brain is not defined, although previous studies suggest that it continues at least up to the beginning of the fourth decade of life (Lebel and Beaulieu, 2011; Somel et al., 2009). Protracted development of brain networks involved in high-order cognition may underpin the emergence of human-specific cognitive abilities (Langer, 2006; Montagu, 1955). Our data suggest that the maturation range may extend to the mid-forties because MT increase in the lateral WM indicates myelin growth up to the age of 45 years, subject to limitations of the cross-sectional design. An MT decrease which follows this estimated end of maturation is also consistent with other findings from animal studies (Peters et al., 2001), showing that lately formed myelin is not stable. As for the onset of cognitive aging, the study by Singh-Maoux et al., (2012) suggests that age-related cognitive decline in

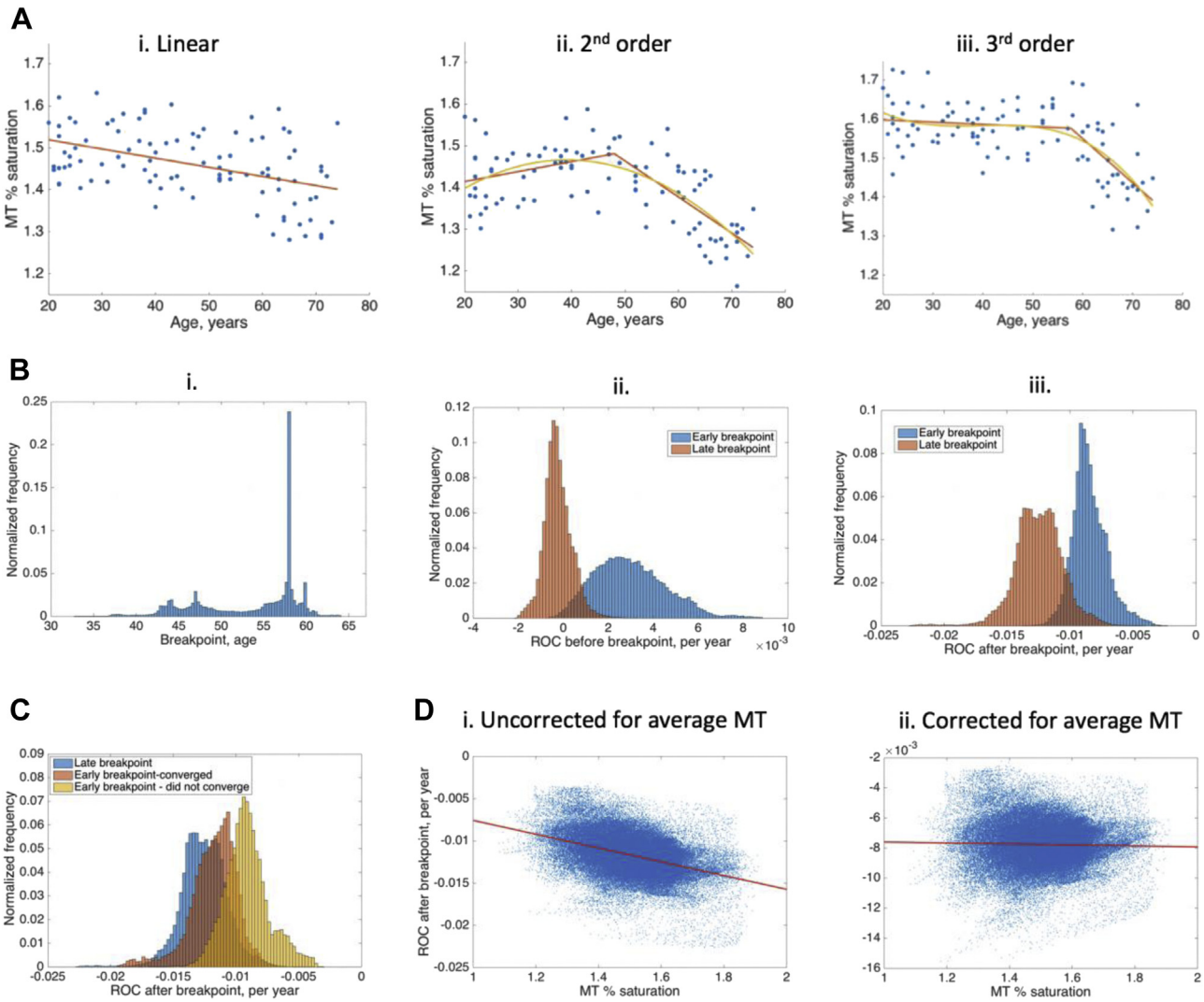

Fig. 5. (A) Examples of fits from representative voxels. (B) A bimodal distribution of breakpoints (i) and their association with rate of change (ROC) before and after the breakpoint (ii-iii). (C) Distributions for 3 sets of voxels at the older age range. (D) Association between average across-subject MT intensity and ROC. Dividing the rate of change by average across-sample MT concentration completely eliminates this association, suggesting a strictly proportional relationship between the two.

high-level cognitive function is detectable from the late forties, whereas other research suggests that impoverished cognitive performance as a result of healthy aging does not occur before the age of 60 years (Hedden and Gabrieli, 2004). Both estimates are consistent with our finding of 2 age-related patterns in the myelin-sensitive maps, that is, a moderate decrease in lateral areas starting in the mid-forties and the onset of a rapid age-related MT decrease in ventral areas in the late fifties.

We also found a few notable deviations from the generic patterns of aging described previously. First, a proportion of voxels showing significant age-related effects were best fitted by the linear model. Second, two—predominantly left-lateralized—areas were better fitted with a two-breakpoint (three-segment) model than a one-breakpoint model. One was situated in the orbitofrontal WM and the other in a segment of the corona radiata, considerably overlapping with the corticospinal tract. These findings warrant further investigation as the age range explored in the present study may have also affected the results, especially in brain areas showing linear patterns of age-related differences. Nonlinear trajectories may have been difficult to identify here simply because none of our participants was old enough to reveal them; a visual inspection of the data shown in Fig. 5A (i) offers some support for this interpretation. The investigation of the extent and configurations of the two-breakpoint patterns would also benefit from an extended age range. However, it is important to note that the finding of patterns which contain an additional early breakpoint are in line with previous studies showing the onset of age-related decrements in some cognitive domains (e.g., perceptual and motor speed) from as early as the 2nd decade of life (Salthouse, 2000).

The cross-sectional design is limited in the conclusions it can draw due to between-subject variability being confounded with aging effects. Longitudinal studies are needed to validate and refine the results reported here (Bender, Völkle, and Raz, 2016). Moreover, we note that the investigation of myelin changes cannot be complete at the mesoscale afforded by the resolution of myelin-sensitive maps and should be complemented with histological studies of the underlying microscale processes (i.e., ballooning, splitting of the myelin sheath).

In conclusion, our novel analyses of MT maps identified and quantified the spatial and temporal features characterizing structural changes in the aging brain at a microstructural level. In addition to the anterior-to-posterior gradient of WM age-related

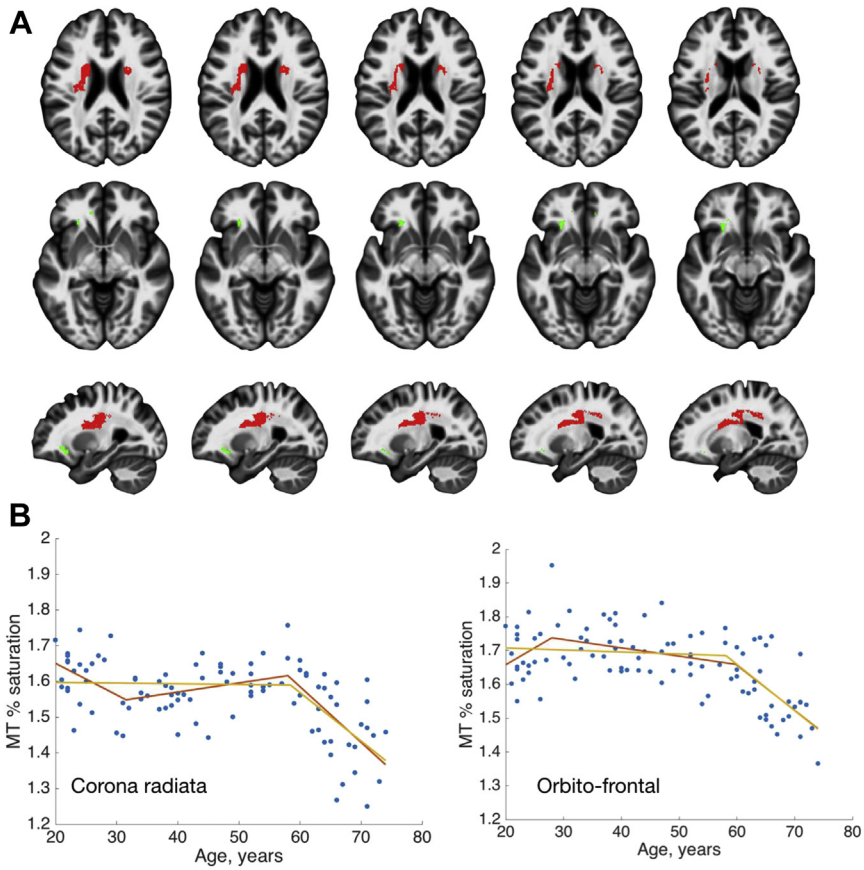

Fig. 6. (A) Two-breakpoint model maps. Left hemisphere is on the left. (B). Examples of one- and two-breakpoint fits from representative voxels in the corona radiata and orbitofrontal white matter.

differences, a lateral-to-ventral gradient was also observed, in line with the temporal sequence of connectivity development and myelogenesis. The temporal characteristics of a lateral-to-ventral gradient did not fit the proposal that areas which mature later decline at an accelerated rate. Instead, brain areas which mature early and show small age-related changes over most of the adult life span demonstrated a rapid MT decrease at a later age.

Disclosure

The authors declare no conflict of interest.

Acknowledgements

This work was supported by a Royal Society Dorothy Hodgkin Fellowship, UK (502008.K518/SLB) (MC) and Royal Society Research Grant, UK (MC), the Wellcome Trust, UK (GR); the European Research Council under the European Union's Seventh Framework Programme (FP7/2007-2013)/ERC grant agreement n° 616905 (NW); the Wellcome Trust Principal Research Fellowship, UK 097720/Z/11/Z, Medical Research Council Project Grant, UK MR/M023672/1, and the Stroke Association Project Grant, UK TSA 2014/02 (TH); The Wellcome Trust Centre for Neuroimaging is supported by core funding from the Wellcome Trust 091593/Z/10/Z.

Appendix A. Supplementary data

Supplementary data to this article can be found online at https://doi.org/10.1016/j.neurobiolaging.2019.03.002.

References

Avants, B.B., Tustison, N.J., Song, G., Cook, P.A., Klein, A., Gee, J.C., 2011. A reproducible evaluation of ANTs similarity metric performance in brain image registration. NeuroImage 54, 2033–2044.
Basser, P.J., Mattiello, J., LeBihan, D., 1994. MR diffusion tensor spectroscopy and imaging. Biophys. J. 66, 259–267.
Bender, A.R., Völkle, M.C., Raz, N., 2016. Differential aging of cerebral white matter in middle-aged and older adults: a seven-year follow-up. NeuroImage 125, 74–83.
Bigler, E.D., Blatter, D.D., Anderson, C.V., Johnson, S.C., Gale, S.D., Hopkins, R.O., Burnett, B., 1997. Hippocampal volume in normal aging and traumatic brain injury. Am. J. Neuroradiol. 18, 11–23.
Brickman, A.M., Meier, I.B., Korgaonkar, M.S., Provenzano, F.A., Grieve, S.M., Siedlecki, K.L., Wasserman, B.T., Williams, L.M., Zimmerman, M.E., 2012. Testing the white matter retrogenesis hypothesis of cognitive aging. Neurobiol. Aging 33, 1699–1715.
Callaghan, M., Freund, P., Draganski, B., Anderson, E., Cappelletti, M., Chowdhury, R., Diedrichsen, J., Fitzgerald, T., Smittenaar, P., Helms, G., Lutti, A., Weiskopf, N., 2014. Wide-spread age-related changes of the microstructure in the human brain revealed by quantitative MRI. Neurobiol. Aging 35, 1862–1872.
Casey, B.J., Giedd, J.N., Thomas, K., 2000. Structural and functional brain development and its relation to cognitive development. Biol. Psychol. 54, 241–257.
Catani, M., Dell'Acqua, F., Vergani, F., Malik, F., Hodge, H., Roy, P., Valabregue, R., Thiebaut de Schotten, M., 2012. Short frontal lobe connections of the human brain. Cortex 48, 273–291.
Davis, S.W., Dennis, N.A., Daselaar, S.M., Fleck, M.S., Cabeza, R., 2008. Qué PASA? The posterior–anterior shift in aging. Cereb. Cortex 18, 1201–1209.
Deoni, S.C., Rutt, B.K., Arun, T., Pierpaoli, C., Jones, D.K., 2008. Gleaning multicomponent T1 and T2 information from steady-state imaging data. Magn. Reson. Med. 60, 1372–1387.
Deoni, S., Mercure, E., Blasi, A., Gasston, D., Thomson, A., Johnson, M., Williams, S., Murphy, D., 2011. Mapping infant brain myelination with magnetic resonance imaging. J. Neurosci. 31, 784–791.
Douaud, G., Jbabdi, S., Behrens, T.E.J., Menke, R.A., Gass, A., Monsch, A., Whitcher, B., Kindlmann, G., Matthews, P.M., Smith, S., 2011. DTI measures in crossing-fibre areas: increased diffusion anisotropy reveals early white matter alteration in MCI and mild Alzheimer's disease. NeuroImage 55, 880–890.

Douaud, G., Groves, A.R., Tamnes, C.K., Westlye, L.T., Duff, E.P., Engvig, A., Walhovd, K.B., James, A., Gass, A., Monschg, A.U., Matthews, P.M., Fjell, A.M., Smith, S.M., Johansen-Berg, H., 2014. A common brain network links development, aging, and vulnerability to disease. Proc. Natl. Acad. Sci. U. S. A. 11, 17648–17653.

Draganski, B., Ashburner, J., Hutton, C., Kherif, F., Frackowiak, R.S.J., Helms, G., Weiskopf, N., 2011. Regional specificity of MRI contrast parameter changes in normal ageing revealed by voxel-based quantification (VBQ). Neuroimage 55, 1423–1434.

Eklund, A., Andersson, M., Josephson, C., Johannesson, M., Knutsson, H., 2012. Does parametric fMRI analysis with SPM yield valid results? - an empirical study of 1484 rest datasets. NeuroImage 61, 565–578.

Fjell, A.M., McEvoy, L., Holland, D., Dale, A.M., Walhovd, K.B., Alzheimer's Disease Neuroimaging Initiative, 2014. What is normal in normal aging? Effects of aging, amyloid and Alzheimer's disease on the cerebral cortex and the hippocampus. Prog. Neurobiol. 117, 20–40.

Flechsig, P., 1901. Developmental (myelogenetic) localisation of the cerebral cortex in the human subject. Lancet 158, 1027–1030.

Folstein, M.F., Folstein, S.E., McHugh, P.R., 1975. 'Mini-mental state'. A practical method for grading the cognitive state of patients for the clinician. J. Psychiatr. Res. 12, 189–198.

Gogtay, N., Giedd, N., Lusk, L., Hayashi, K., Greenstein, D., Vaituzis, A., Nugent, T.F.I.I.I., Herman, D.H., Clasen, L.S., Toga, A.W., Rapoport, J.L., Thompson, P.M., 2004. Dynamic mapping of human cortical development during childhood through early adulthood. Proc. Natl. Acad. Sci. U. S. A. 101, 8174–8179.

Head, D., Buckner, R.L., Shimony, J.S., Williams, L.E., Akbudak, E., Conturo, T.E., McAvoy, M., Morris, J.C., Snyder, A.Z., 2004. Differential vulnerability of anterior white matter in nondemented aging with minimal acceleration in dementia of the Alzheimer type: evidence from diffusion tensor imaging. Cereb. Cortex 14, 410–423.

Hedden, T., Gabrieli, J.D.E., 2004. Insights into the ageing mind: a view from cognitive neuroscience. Nat. Rev. Neurosci. 5, 87–96.

Helms, G., Dathe, H., Kallenberg, K., Dechent, P., 2008. High-resolution maps of magnetization transfer with inherent correction for RF inhomogeneity and T1 relaxation obtained from 3D FLASH MRI. Magn. Reson. Med. 60, 1396–1407.

Huang, J., Friedland, R.P., Auchus, A.P., 2007. Diffusion tensor imaging of normal-appearing white matter in mild cognitive impairment and early Alzheimer disease: preliminary evidence of axonal degeneration in the temporal lobe. Am. J. Neuroradiology 28, 1943–1948.

Jones, D.K., Knösche, T.K., Turner, R., 2012. White matter integrity, fiber count, and other fallacies: the do's and don'ts of diffusion MRI. NeuroImage 73, 239–254.

Keihaninejad, S., Heckemann, R.A., Fagiolo, G., Symms, M.R., Hajnal, J.V., Hammers, A., The Alzheimer's Disease Neuroimaging Initiative, 2010. A robust method to estimate the intracranial volume across MRI field strengths (1.5T and 3T). Neuroimage 50, 1427–1437.

Kinney, H.C., Brody, B.A., Kloman, A.S., Gilles, F.H., 1988. Sequence of central nervous system myelination in human infancy. II. Patterns of myelination in autopsied infants. J. Neuropathol. Exp. Neurol. 47, 217–234.

Klein, A., Andersson, J., Ardekani, B.A., Ashburner, J., Avants, B., Chiang, M.C., Christensen, G.E., Collins, D.L., Gee, J., Hellier, P., Song, J.H., Jenkinson, M., Lepage, C., Rueckert, D., Thompson, P., Vercauteren, T., Woods, R.P., Mann, J.J., Parsey, R.V., 2009. Evaluation of 14 nonlinear deformation algorithms applied to human brain MRI registration. Neuroimage 46, 786–802.

Knutsson, H., Westin, C.F., 1993. Normalized and differential convolution: methods for interpolation and filtering of incomplete and uncertain data. Proc. IEEE Comput. Vis. Pattern Recognit. 515–523.

Kostovic, I., Jovanov-Milošević, N., 2006. The development of cerebral connections during the first 20–45 weeks' gestation. Semin. Fetal Neonatal Med. 11, 415–422.

Langer, J., 2006. The heterochronic evolution of primate cognitive development. Biol. Theory 1, 41–43.

Lebel, C., Beaulieu, C., 2011. Longitudinal development of human brain wiring continues from childhood into adulthood. J. Neurosci. 31, 10937–10947.

Lee, J.E., Chung, M.K., Lazar, M., DuBray, M.B.A., Kim, J., Bigler, E.D., Lainhart, J.E., Alexander, A.L., 2009. Study of diffusion tensor imaging by tissue-specific, smoothing-compensated voxel-based analysis. NeuroImage 44, 870–883.

Lutti, A., Hutton, C., Finsterbusch, J., Helms, G., Weiskopf, N., 2010. Optimization and validation of methods for mapping of the radiofrequency transmit field at 3T. Magn. Reson. Med. 64, 229–238.

Lutti, A., Stadler, J., Josephs, O., Windischberger, C., Speck, O., Bernarding, J., Hutton, C., Weiskopf, N., 2012. Robust and fast whole brain mapping of the RF transmit field B1 at 7T. PLoS One 7, e32379.

Montagu, M.F.A., 1955. Time, morphology, and neoteny in the evolution of man. Am. Anthropol. 57, 13–27.

Ou, X., Sun, S.-W., Liang, H.-F., Song, S.-K., Gochber, D.F., 2009. Quantitative magnetization transfer measured pool-size ratio reflects optic nerve myelin content in ex vivo mice. Magn. Reson. Med. 61, 364–371.

Owen, A.M., McMillan, K.M., Laird, A.R., Bullmore, E., 2005. N-back working memory paradigm: a meta-analysis of normative functional neuroimag- ing studies. Hum. Brain Mapp. 25, 46–59.

Peters, A., Sethares, C., Killiany, R.J., 2001. Effects of age on the thickness of myelin sheaths in monkey primary visual cortex. J. Comp. Neurol. 435, 241–248.

R Development Core Team, 2015. R: A Language and Environment for Statistical Computing. R Foundation for Statistical Computing, Vienna, Austria. Available at: https://www.R-project.org. (Accessed 20 May 2016).

Raz, N., 2000. Aging of the brain and its impact on cognitive performance: integration of structural and functional finding. In: Craik, F., Salthouse, T. (Eds.), Handbook of Aging and Cognition II. Erlbaum, Mahwah, NJ, pp. 1–90.

Raz, N., Gunning, F.M., Head, D., Dupuis, J.H., McQuain, J., Briggs, S.D., Loken, W.J., Thornton, A.E., Acker, J.D., 1997. Selective aging of the human cerebral cortex observed in vivo: differential vulnerability of the prefrontal gray matter. Cereb. Cortex 7, 268–282.

Raz, N., Gunning-Dixon, F.M., Head, D., Dupuis, J.H., Acker, J.D., 1998. Neuroanatomical correlates of cognitive aging: evidence from structural magnetic resonance imaging. Neuropsychology 12, 95–114.

Raz, N., Lindenberger, U., Rodrigue, K.M., Kennedy, K.M., Head, D., Williamson, A., Dahle, C., Gerstorf, D., Acker, J.D., 2005. Regional brain changes in aging healthy adults: general trends, individual differences and modifiers. Cereb. Cortex 15, 1676–1689.

Reisberg, B., Franssen, E.H., Hasan, S.M., Monteiro, I., Boksay, I., Souren, L.E., Kenowsky, S., Auer, S.R., Elahi, S., Kluger, A., 1999. Retrogenesis: clinical, physiologic, and pathologic mechanisms in brain aging, Alzheimer's and other dementing processes. Eur. Arch. Psychiatry Clin. Neurosci. 3, 28–36.

Rivers, L., Young, K.M., Rizzi, M., Jamen, F., Psachoulia, K., Wade, A., Kessaris, N., Richardson, W.D., 2008. PDGFRA/NG2 glia generate myelinating oligodendrocytes and piriform projection neurons in adult mice. Nat. Neu 11, 1392–1401.

Salat, D.H., Tuch, D.S., Greve, D.N., van der Kouwe, A.J., Hevelone, N.D., Zaleta, A.K., Rosen, B.R., Fischl, B., Corkin, S., Rosas, H.D., Dale, A.M., 2005a. Age-related alterations in white matter microstructure measured by diffusion tensor imaging. Neurobiol. Aging 26, 1215–1227.

Salat, D.H., Tuch, D.S., Hevelone, N.D., Fischl, B., Corkin, S., Rosas, H.D., Dale, A.M., 2005b. Age-related changes in prefrontal white matter measured by diffusion tensor imaging. Ann. N. Y. Acad. Sci. 1064, 37–49.

Salthouse, T.A., 2000. Aging and measures of processing speed. Biol. Psychol. 54, 35–54.

Schmierer, K., Tozer, D.J., Scaravilli, F., Altmann, D.R., Barker, G.J., Tofts, P.S., Miller, D.H., 2007. Quantitative magnetization transfer imaging in postmortem multiple sclerosis brain. J. Magn. Reson. Imaging 26, 41–51.

Schmierer, K., Wheeler-Kingshott, C.A.M., Tozer, D.J., Boulby, P.A., Parkes, H.G., Yousry, T.A., Scaravilli, F., Barker, G.J., Tofts, P.S., Miller, D.H., 2008. Quantitative magnetic resonance of postmortem multiple sclerosis brain before and after fixation. Magn. Reson. Med. 59, 268–277.

Schmitz, T.W., Spreng, N., The Alzheimer's Disease Neuroimaging Initiative, 2016. Basal forebrain degeneration precedes and predicts the cortical spread of Alzheimer's pathology. Nat. Commun. 7, 13249.

Sexton, C.E., Walhovd, K.B., Storsve, A.B., Tamnes, C.K., Westlye, L.T., Johansen-Berg, H., Fjell, A.M., 2014. Accelerated changes in white matter microstructure during aging: a longitudinal diffusion tensor imaging study. J. Neurosci. 34, 15425–15436.

Shaw, P., Kabani, N.J., Lerch, J.P., Eckstrand, K., Lenroot, R., Gogtay, N., Greenstein, D., Clasen, L., Evans, A., Rapoport, J.L., Giedd, J.N., Wise, S.P., 2008. Neurodevelopmental trajectories of the human cerebral cortex. J. Neurosci. 28, 3586–3594.

Singh-Manoux, A., Kivimaki, M., Glymour, M.M., Elbaz, A., Berr, C., Ebmeier, K.P., Ferrie, J.E., Dugravot, A., 2012. Timing of onset of cognitive decline. BMJ 344, d7622.

Somel, M., Franz, H., Yan, Z., Lorenc, A., Guo, S., Giger, T., Kelso, J., Nickel, B., Dannemann, M., Bahn, S., Webster, M.J., Weickert, C.S., Lachmann, M., Pääbo, S., Khaitovich, P., 2009. Transcriptional neoteny in the human brain. Proc. Natl. Acad. Sci. U. S. A. 106, 5743–5748.

Sowell, E.R., Peterson, B.S., Thompson, P.M., Welcome, S.E., Henkenius, A.L., Toga, A.W., 2003. Mapping cortical change across the human life span. Nat. Neurosci. 6, 309–315.

Sowell, E.R., Thompson, P.M., Leonard, C.M., Welcome, S.E., Kan, E., Toga, A.W., 2004. Longitudinal mapping of cortical thickness and brain growth in normal children. J. Neurosci. 24, 8223–8231.

Sturm, V.E., Yokoyama, J.S., Seeley, W.W., Kramer, J.K., Miller, B.L., Rankin, K.P., 2013. Heightened emotional contagion in mild cognitive impairment and Alzheimer's disease is associated with temporal lobe degeneration. Proc. Natl. Acad. Sci. U. S. A. 110, 9944–9949.

Toms, J.D., Lesperance, M.L., 2003. Piecewise regression: a tool for identifying ecological thresholds. Ecology 84, 2034–2041.

Weiskopf, N., Suckling, J., Williams, G., Correia, M.M., Inkster, B., Tait, R., Ooi, C., Bullmore, E.T., Lutti, A., 2013. Quantitative multi-parameter mapping of R1, PD*, MT, and R2* at 3T: a multi-center validation. Front. Neurosci. 7, 1–11.

West, M.J., Coleman, P.D., Flood, D.G., Troncoso, J.C., 1994. Differences in the pattern of hippocampal neuronal loss in normal ageing and Alzheimer's disease. Lancet 8925, 769–772.

Wisse, L., Biessels, G.J., Heringa, S.M., Kuijf, H.J., Dineke, H., Koekd, L., Luijtene, P.R., Geerlings, M.I., 2014. On behalf of the Utrecht Vascular Cognitive Impairment (VCI). Hippocampal subfield volumes at 7T in early Alzheimer's disease and normal aging. Neurobiol. Aging 35, 2039–2045.

Yakovlev, P.I., Leours, A.R., 1967. The myelogenetic cycles of regional maturation of the brain. In: Minkowski, A. (Ed.), Regional Development of the Brain in Early Life. Blackwell, Oxford, pp. 3–70.